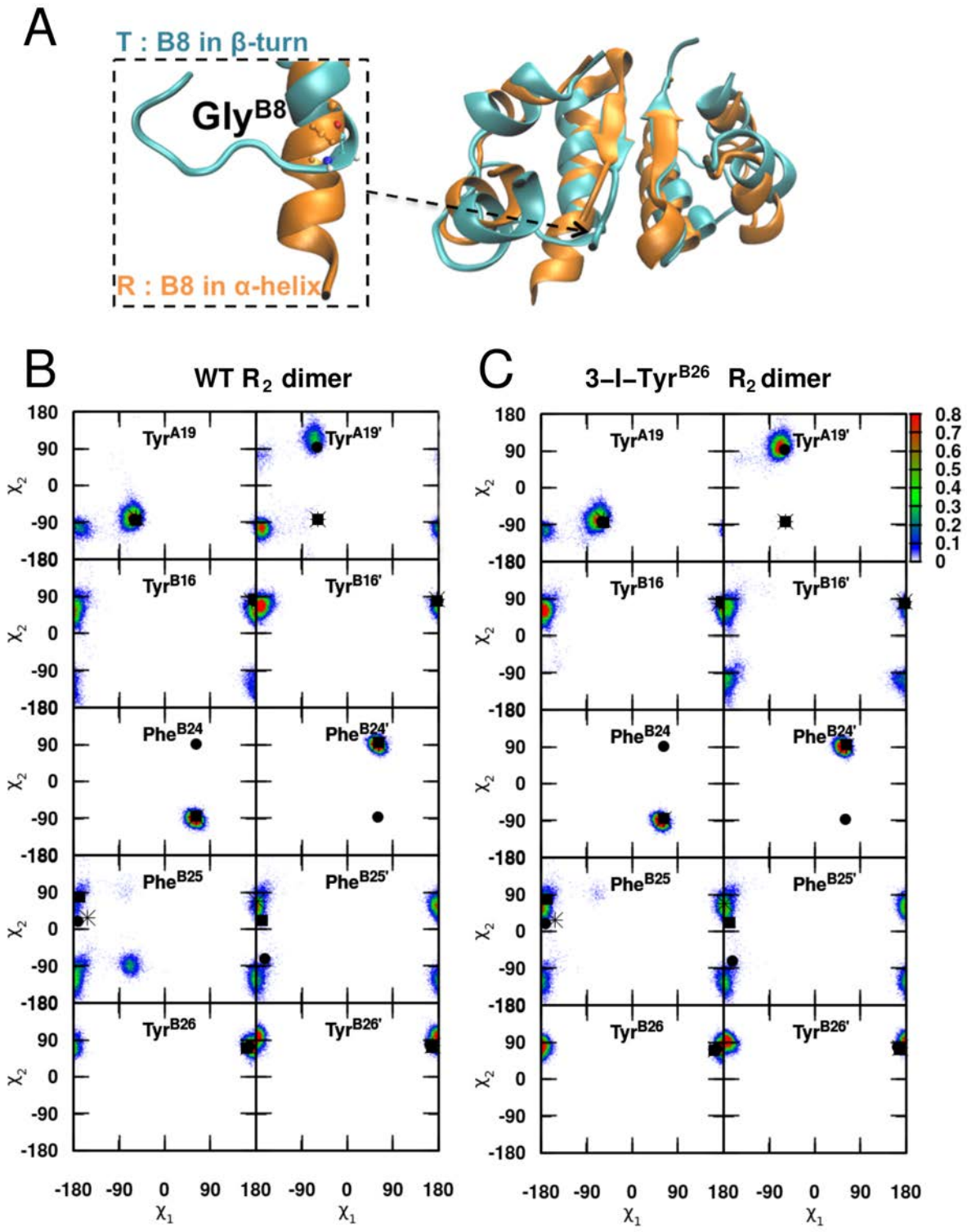

FIGURE S1. **Dihedral probability distribution functions for the R_2 dimers.** (*A*) Structure of the R- (α-helix B1-B8; *gold*) and T (disordered strand B1-B8; *cyan*) -states of insulin dimer. The *inset* indicates the placement of the invariant Gly^{B8} as a function of T/R state. Only Gly^{B8} is illustrated. (*B* and *C*) Probability distribution functions $P(\chi_1,\chi_2)$ for Tyr^{A19}, Tyr^{B16}, Phe^{B24}, Phe^{B25}, Tyr^{B26} and their dimer related mates (indicated by *primes*) for (*B*) the WT R_2 insulin dimer, and (*C*) the 3-iodo-Tyr^{B26} R_2 insulin dimer. The distributions were built from 20 ns equilibrium MD simulations. The starting dimer structure was taken from a dimer of WT R_6 zinc

insulin crystal structure (PDB code 1ZNJ). Symbols (*box, star, circle*) indicate positions in the X-ray crystal structure of the 3-I-Tyr^{B26}-Nle^{B29}–insulin hexamer.

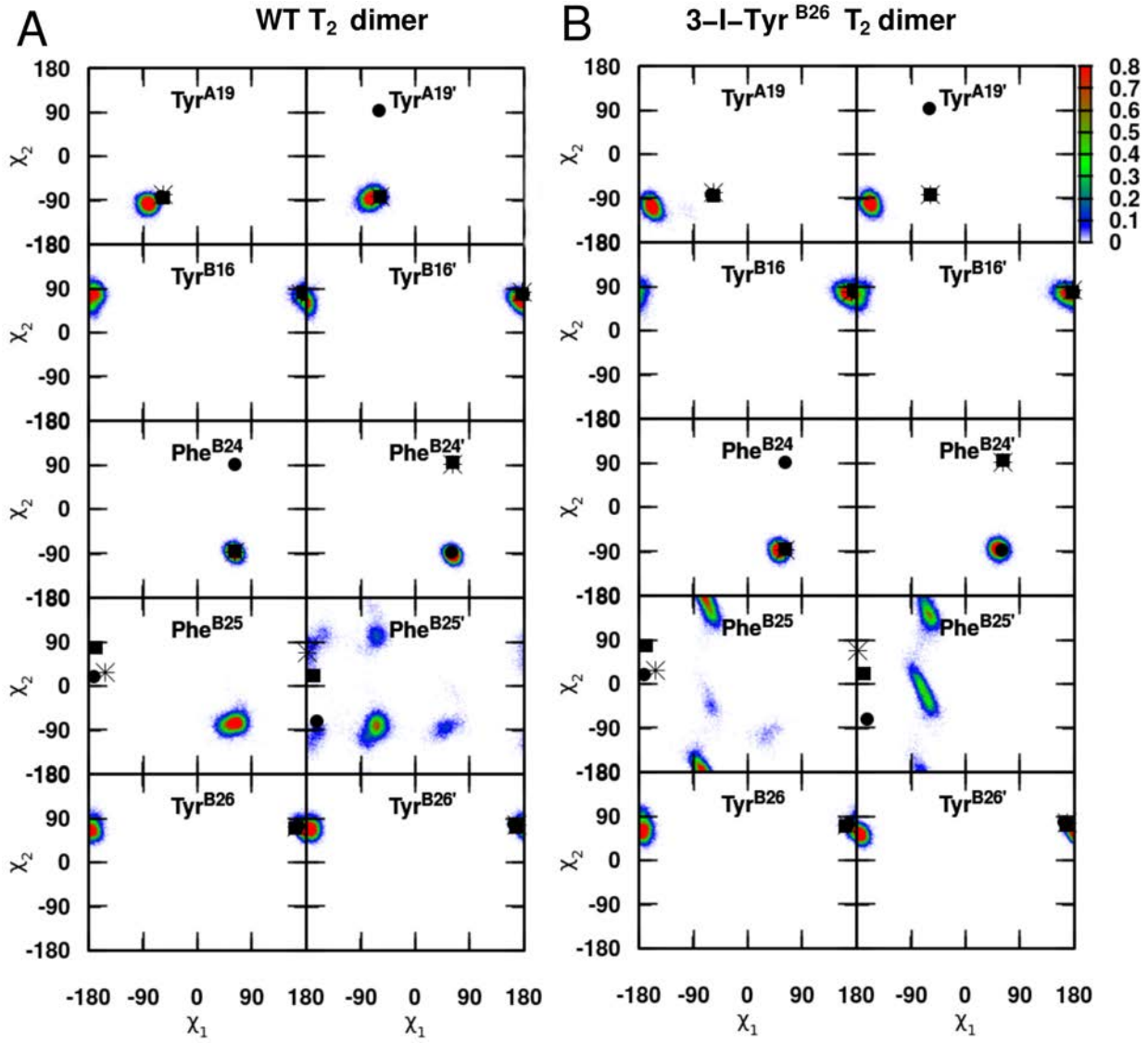

FIGURE S2. **Dihedral probability distribution functions for the T_2 dimers.** Probability distribution functions $P(\chi_1,\chi_2)$ for Tyr^{A19}, Tyr^{B16}, Phe^{B24}, Phe^{B25}, Tyr^{B26} and their dimer-related mates (indicated by *primes*) for (*A*) the WT T_2 dimer, and (*B*) the 3-iodo-Tyr^{B26} T_2 dimer. The distributions were built from 20 ns of equilibrium MD simulations. The starting dimer structure was taken from the T_2 zinc-free dimer WT-insulin structure (PDB code 1DPH). Symbols (*box, star,* and *circle*) indicate positions in the X-ray crystal structure of the 3-I-Tyr^{B26}-Nle^{B29}-insulin hexamer. The side chain of Phe^{B25} is disordered; see main text.

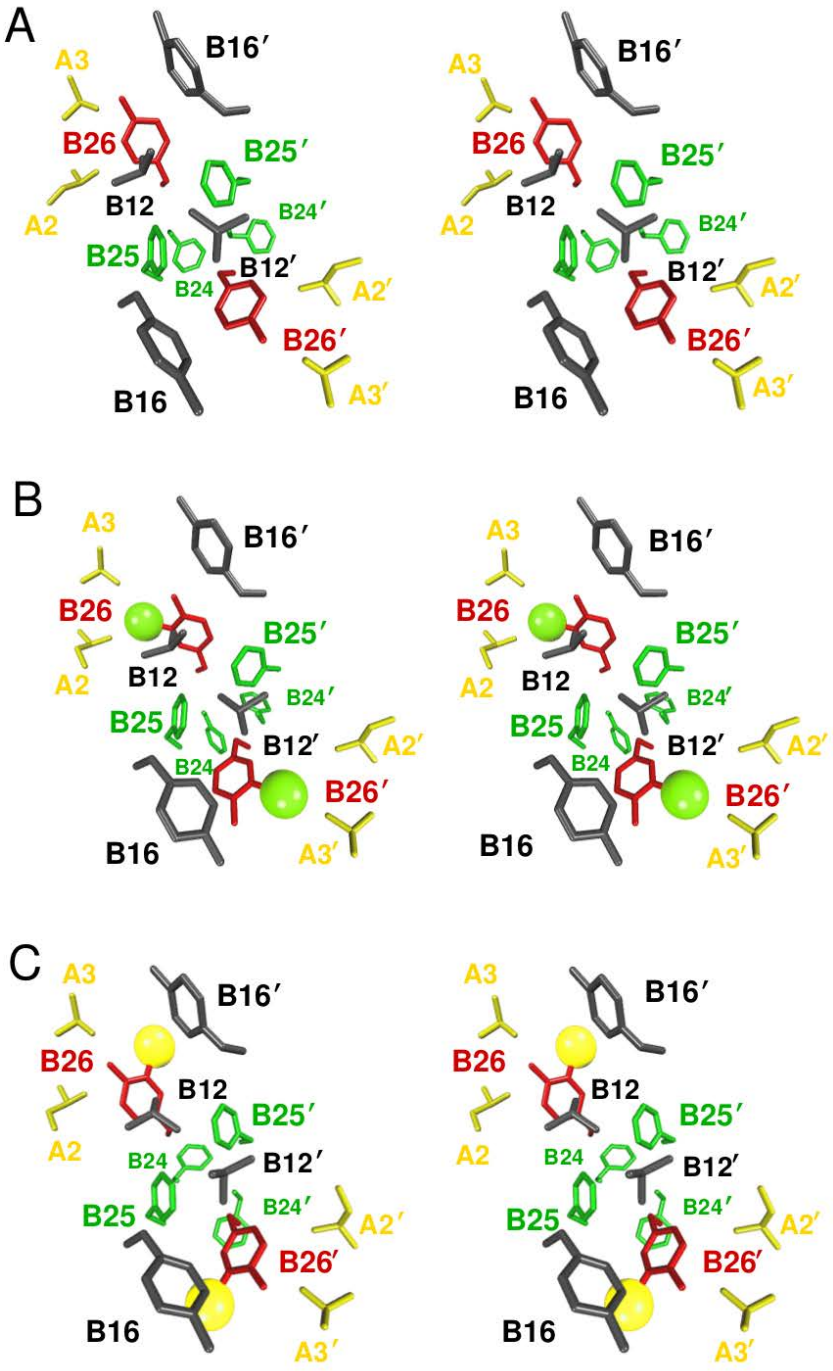

FIGURE S3. **Packing prediction at the dimer interface.** Stereo view of the predicted conformational maps of B-chain aromatic residues from 20 ns MD simulation: (*A*) Packing in the WT-, (*B*) 3-I-Tyr^{B26}- and (*C*) 5-I-Tyr^{B26}-insulin dimers. Residues Ile^{A2}, Val^{A3}, Val^{B12}, Tyr^{B16}, Phe^{B24}, Phe^{B25}, and Tyr^{B26} are shown explicitly (in *licorice*) together with their dimer-related mates. Note the displacement of Val^{B12} in (*C*) due to 5-I-Tyr^{B26}, compared to WT- and 3-I-Tyr^{B26} dimers (see main text). The starting dimer structures were taken from the T_2 zinc-free dimer WT-insulin structure (PDB code 1DPH). The iodine atoms are shown as *green* and *yellow* spheres for 3-I-Tyr^{B26}- and (*C*) 5-I-Tyr^{B26} -insulin dimers, respectively. For an overall view, see also Figure S4.

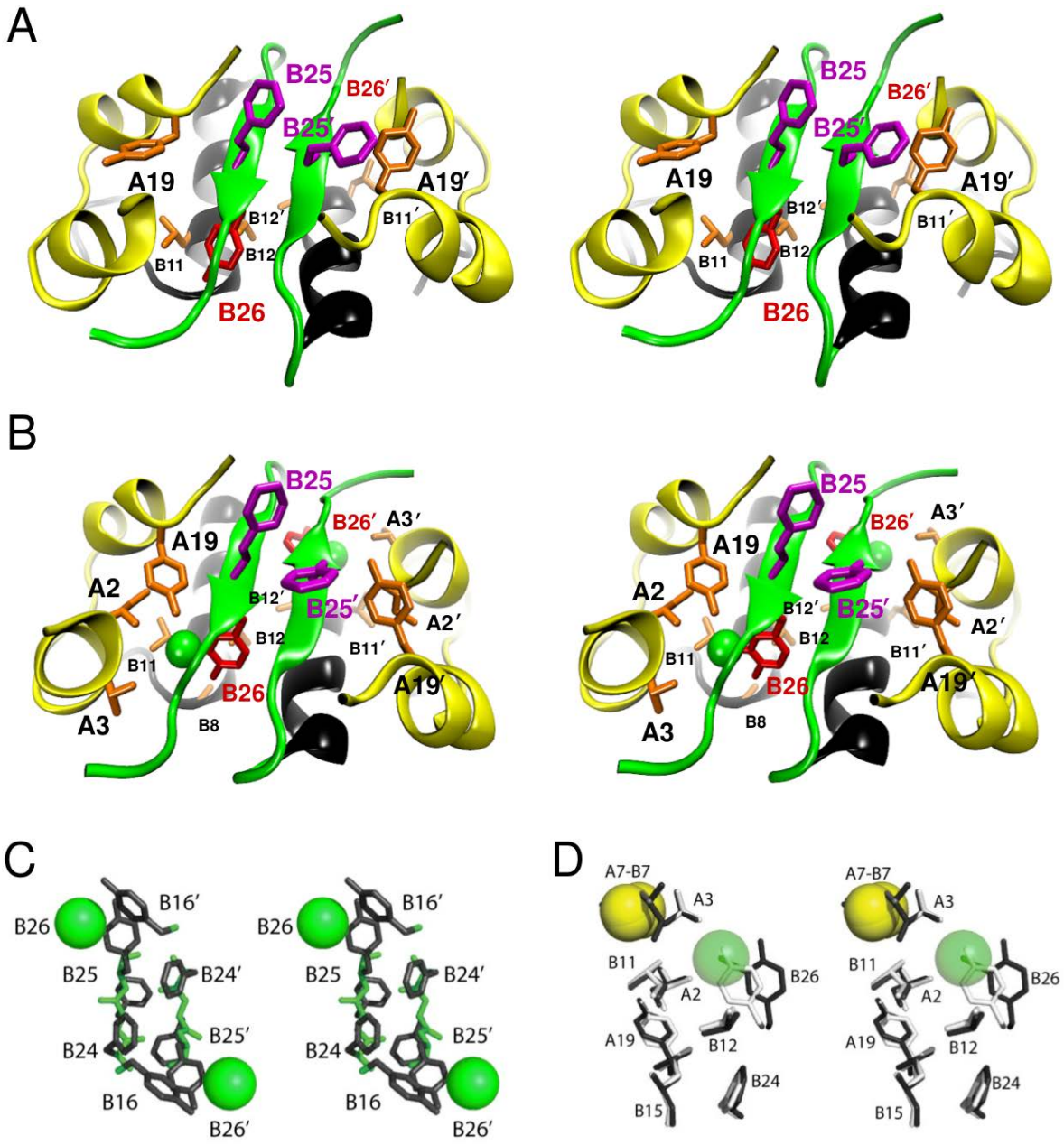

FIGURE S4. **Packing at the dimer interface of 3-I-Tyr^{B26} insulin analog: predicted (A,B) vs. crystal structure (C, D) .** (*A*) WT dimer: Residues Val^{B12}, Tyr^{A19}, Phe^{B25}, and Tyr^{B26} are shown (in *licorice*) together with dimer-related mates. (*B*) 3-I-Tyr^{B26} dimer: Local interactions with residue Ile^{A2}, Val^{A3}, Gly^{B8}, Leu^{B11}, Val^{B12}, and Tyr^{A19} are explicitly shown. Iodine atoms are shown as *green* spheres. For a simplified view, see also Figure S3. (*C*) Stereo view of aromatic-rich dimer interface. The side chains of Tyr^{B16}, Phe^{B24}, Phe^{B25} and 3-I-Tyr^{B26} (*dark gray* sticks) are shown in relation to their dimer-related partners and a portion of the anti-parallel β-sheet (*green*; main chain of residues B24-B26 and B24'-B26'). (*D*) Expanded view of corresponding WT and variant B26 side-chain environments in relation to an inter-chain crevice containing Ile^{A2}, Val^{A3} and Val^{B12}. Neighboring side chains are as labeled; the sulfur atoms of cystine A7-B7 are shown as *yellow* spheres (van der Waals radii). WT coordinates for panels *C* and *D* were obtained from PDB entry 1ZNJ.

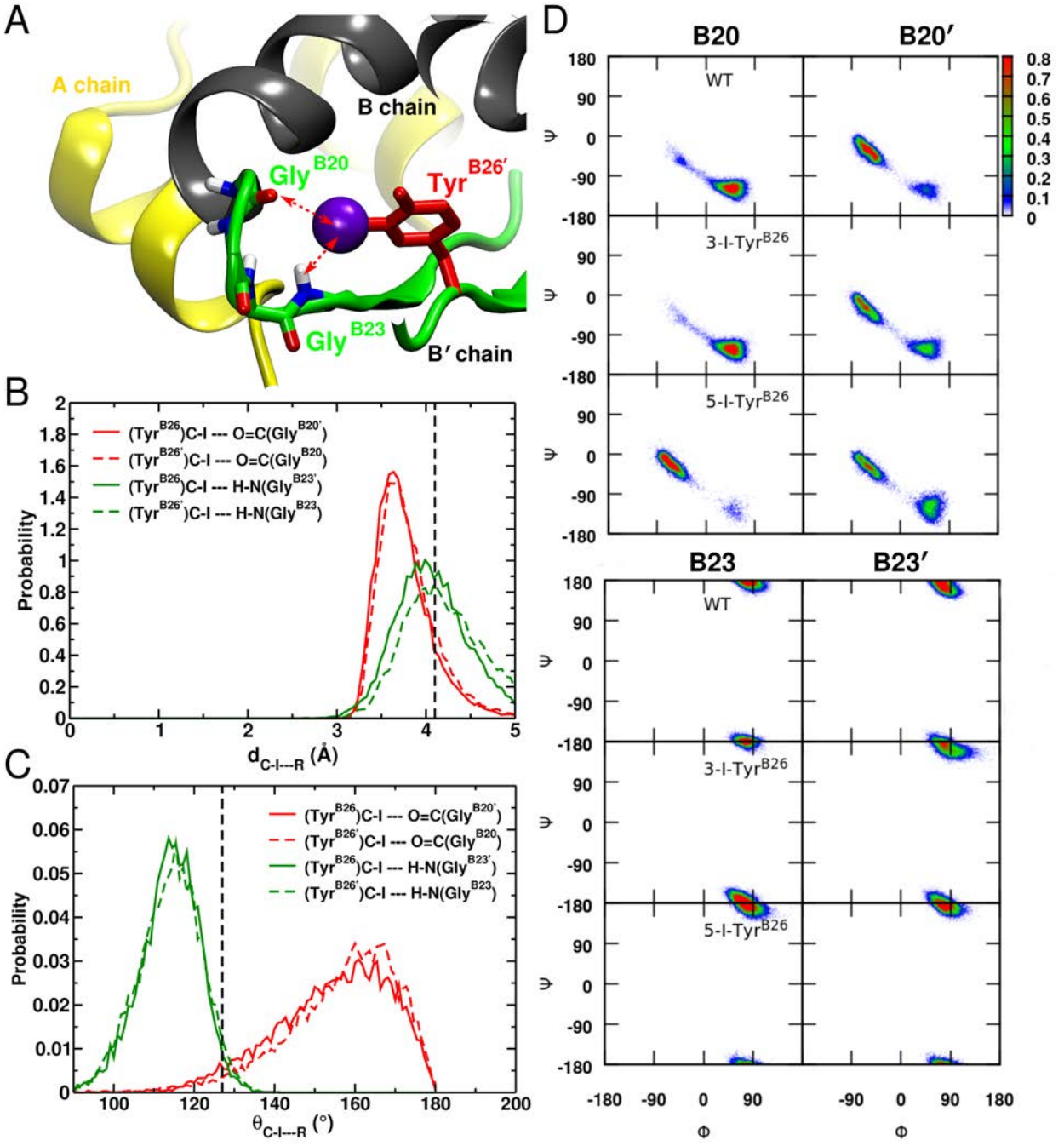

FIGURE S5. **5-I-Tyr^{B26}-insulin dimerization interface.** (*A*) Structure of 5-I-Tyr$^{B26'}$-insulin monomer packing against its related partner illustrates local interaction network between iodine on Tyr$^{B26'}$ and the backbone oxygen of Gly^{B20} and the backbone NH of Gly^{B23}. The iodine atom is shown as a *purple* sphere. Only residues interacting with 5-I-Tyr$^{B26'}$ are illustrated. Potential hydrogen/halogen bonds with I are shown as *dashed red lines*. (*B*) Distance probability distribution of I(Tyr^{B26})—O(Gly$^{B20'}$) (*solid red*), I(Tyr$^{B26'}$)—O(Gly^{B20}) (*dashed red*), I(Tyr^{B26})—HN(Gly$^{B23'}$) (*solid green*), and I(Tyr$^{B26'}$)—HN(Gly^{B23}) (*dashed green*) from 20 ns of MD simulation. The *black dashed line* at 4.1 Å represents the I—O distance interaction limit. (*C*) Angle probability distribution of C-I(Tyr^{B26})—O(Gly$^{B'20'}$) (*solid red*), C-I(Tyr$^{B26'}$)—O(Gly^{B20}) (*dashed red*), C-I(Tyr^{B26})—HN(Gly$^{B23'}$) (*solid green*), and C-I(Tyr$^{B26'}$)—HN(Gly^{B23}) (*dashed green*) from 20 ns MD simulation. The *black dashed line* at 127° represents the angular limit for I between negative electrostatic region ($\delta^- < 127°$) and positive electrostatic region ($127° < \delta^+ <$

233°). (*D*) Predicted backbone dihedral angle distributions (ϕ, ψ) of Gly^{B20} (*upper* panels) and Gly^{B23} (*lower* panels) in the B20-B23 β-turn in WT, 3-I-Tyr^{B26} and 5-I-Tyr^{B26} insulin dimer from 20 ns of MD simulation, and compared to their dimer-related partners (indicated by primes). The starting dimer structure was taken from the T_2 Zinc-free dimer WT-insulin structure (PDB code 1DPH). 5-I-Tyr^{B26} dimer exhibit increased interaction energy along the dimerization interface, compared to WT and 3-I-Tyr^{B26}, but note that the way iodine interacts with the backbone O(Gly^{B20}) leads to its accommodation in a region in the Ramachandran plot that is in principle permitted for glycine but which is empirically unfavorable in the context of the native conformation of insulin (Nakagawa, S. Hua, Q.-X., Jia, W., Wang, S., Katsoyannis, P.G. and Weiss, M.A. (2006) Chiral Mutagenesis of Insulin. CONTRIBUTION OF THE B20-B23 β-TURN TO ACTIVITY AND STABILITY. *J. Biol. Chem*. **281**, 22386-96).

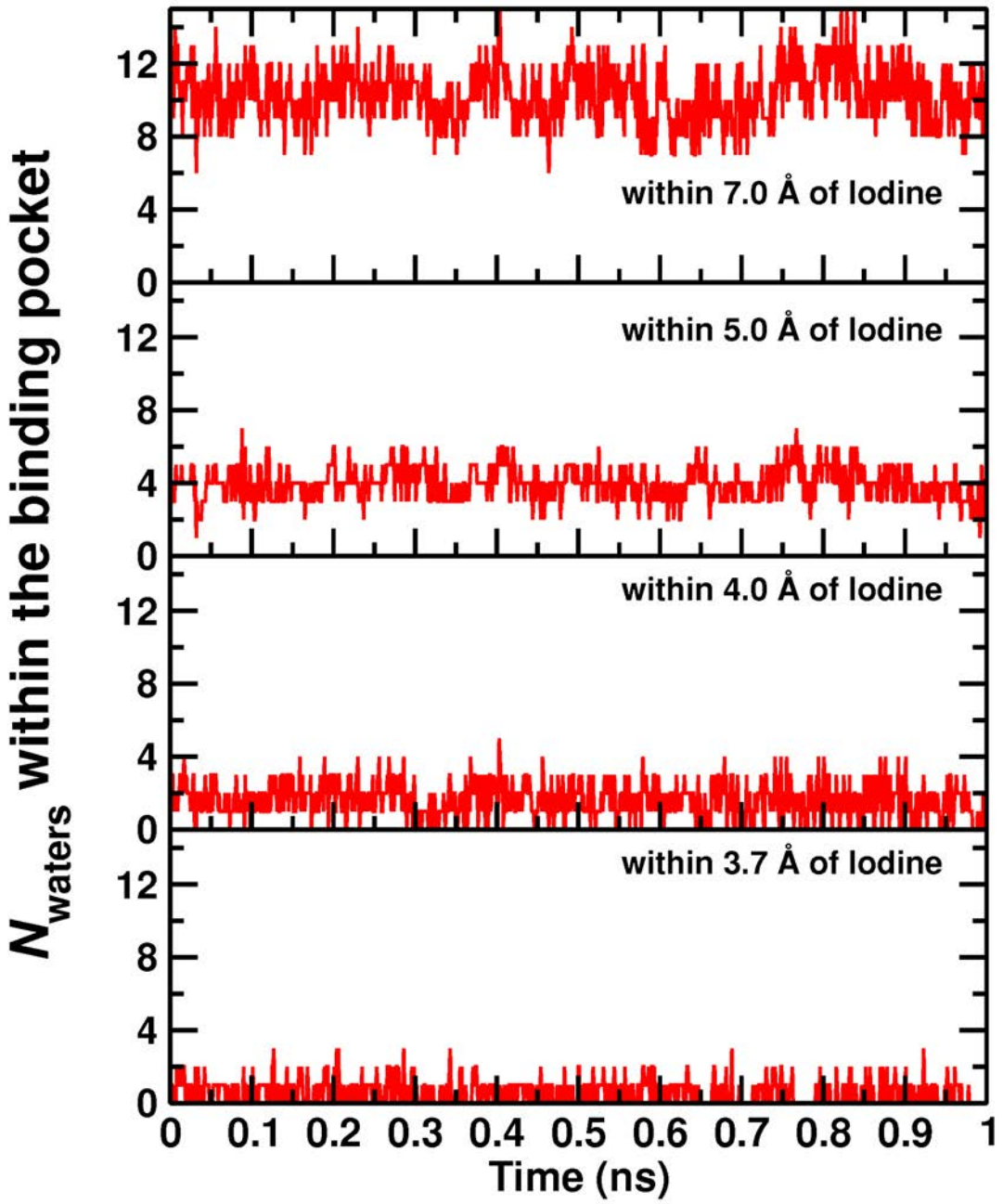

FIGURE S6. **Population of water molecules at the 3-I-Tyr^{B26}/μIR interface.** The number *N* of water molecules present in a 3.7, 4.0, 5.0 and 7.0 Å spheres centered around the iodine atom within the 3-I-Tyr^{B26}/μIR binding pocket during the 1 ns MD simulations.

Table S1. Iodo-Tyr^{B26} –induced interaction energies contributing to the dimerization. Interaction energies E_{total} (sum of van der Waals, E_{vdW}, and electrostatic, E_{elec}, terms) between Tyr^{B26} and neighboring residues calculated for both PC (A) and MTP (B) electrostatics.

(A)

$\mathbf{E}_{inter}$	3-I-Tyr^{B26}			5-I-Tyr^{B26}		
(kcal/mol)	$\mathbf{E}_{vdW}$	$\mathbf{E}_{elec}$	$\mathbf{E}_{total}$	$\mathbf{E}_{vdW}$	$\mathbf{E}_{elec}$	$\mathbf{E}_{total}$
Ile^{A2}	-1.25	-0.06	-1.31	-0.87	-0.02	-0.90
Leu^{A3}	-0.89	-0.18	-1.07	-0.46	-0.18	-0.65
Gly^{B8}	-1.52	-0.41	-1.93	-0.98	0.06	-0.92
Leu^{B11}	-0.94	-0.49	-1.42	-1.13	-0.47	-1.60
Val^{B12}	-2.45	-0.36	-2.81	-2.38	-0.37	-2.75
Leu^{B15}	-0.85	0.02	-0.83	-0.91	0.02	-0.89
Pro^{B28}	-3.53	-0.09	-3.63	-3.23	-0.09	-3.32
Tyr$^{B16'}$	-2.34	-0.89	-3.23	-2.60	-0.32	-2.92
Gly$^{B20'}$	-0.74	-1.77	-2.51	-0.33	-0.04	-0.38
Gly$^{B23'}$	-1.06	0.84	-0.22	-1.39	0.31	-1.08
Phe$^{B24'}$	-2.62	-0.68	-3.30	-3.47	-0.64	-4.11
Total	-18.19	-4.06	-22.25	-17.75	-1.75	-19.50

(B)

$\mathbf{E}_{inter}$	3-I-Tyr^{B26}			5-I-Tyr^{B26}		
(kcal/mol)	$\mathbf{E}_{vdW}$	$\mathbf{E}_{elec}$	$\mathbf{E}_{total}$	$\mathbf{E}_{vdW}$	$\mathbf{E}_{elec}$	$\mathbf{E}_{total}$
Ile^{A2}	-0.95	-0.47	-1.41	-0.54	-0.39	-0.94
Leu^{A3}	-0.84	-0.34	-1.17	-0.29	-0.30	-0.59
Gly^{B8}	-1.31	0.57	-0.73	-0.54	-0.01	-0.55
Leu^{B11}	-0.94	-0.63	-1.58	-0.66	-0.46	-1.12
Val^{B12}	-2.39	-0.91	-3.30	-2.04	-0.83	-2.87
Leu^{B15}	-0.78	-0.41	-1.19	-0.74	-0.38	-1.12
Pro^{B28}	-3.10	-0.89	-3.99	-2.24	-0.78	-3.02
Tyr$^{B16'}$	-2.52	-1.39	-3.91	0.28	-1.96	-1.68
Gly$^{B20'}$	-0.60	-0.92	-1.52	-0.74	-1.73	-2.47
Gly$^{B23'}$	-0.96	-0.60	-1.56	-0.73	-2.16	-2.89
Phe$^{B24'}$	-2.95	-0.02	-2.97	-2.15	-0.14	-2.29
Total	-17.32	-6.01	-23.33	-10.39	-9.14	-19.53